Mon. Not. R. Astron. Soc. **320**, 424–434 (2001)

The Galactic disc distribution of planetary nebulae with warm dust emission features – I

S. Casassus,[1,2] P. F. Roche,[1★] D. K. Aitken[3] and C. H. Smith[4]
[1]*Astrophysics, Physics Department, Oxford University, Keble Road, Oxford OX1 3RH*
[2]*Departamento de Astronomía, Universidad de Chile, Casilla 36-D, Santiago, Chile*
[3]*Department of Physical Sciences, University of Hertfordshire, Hatfield, Herts AL10 9AB*
[4]*School of Physics, University College, UNSW, Canberra, ACT 2600, Australia*

Accepted 2000 July 14. Received 2000 June 30; in original form 2000 March 17

ABSTRACT

We investigate the Galactic disc distribution of a sample of planetary nebulae characterized in terms of their mid-infrared spectral features. The total number of Galactic disc PNe with 8–13 μm spectra is brought up to 74 with the inclusion of 24 new objects, the spectra of which we present for the first time. 54 PNe have clearly identified warm dust emission features, and form a sample that we use to construct the distribution of the C/O chemical balance in Galactic disc PNe. The dust emission features complement the information on the progenitor masses brought by the gas-phase N/O ratios: PNe with unidentified infrared emission bands have the highest N/O ratios, while PNe with the silicate signature have either very high N enrichment or close to none. We find a trend for a decreasing proportion of O-rich PNe towards the third and fourth Galactic quadrants. Two independent distance scales confirm that the proportion of O-rich PNe decreases from 30 ± 9 per cent inside the solar circle to 14 ± 7 per cent outside. PNe with warm dust are also the youngest. PNe with no warm dust are uniformly distributed in C/O and N/O ratios, and do not appear to be confined to $\mathrm{C/O} \sim 1$. They also have higher 6-cm fluxes, as expected from more evolved PNe. We show that the *IRAS* fluxes are a good representation of the bolometric flux for compact and IR-bright PNe, which are probably optically thick. Selection of objects with $F(12\,\mu\mathrm{m}) > 0.5$ Jy should probe a good portion of the Galactic disc for these young, dense and compact nebulae, and the dominant selection effects are rooted in the PN catalogues.

Key words: ISM: abundances – planetary nebulae: general – infrared: ISM.

1 INTRODUCTION

Spectroscopy at 10 μm has brought significant information on the chemical composition of planetary nebulae (PNe). The dust signatures reflect the C/O chemical balance at the tip of the asymptotic giant branch (AGB). In this paper we use the 8–13 μm dust signatures as a systematic tool to investigate the distribution of the C/O abundance ratio in PNe. We classify the 8–13 μm spectral signatures in a sample consisting of all compact and IR-bright PNe in the Strasbourg-ESO catalogue (Acker et al. 1992). The sample excludes PNe traditionally associated with the Galactic bulge, which will be the subject of a forthcoming paper.

The family of emission bands usually referred to as the 'unidentified infrared bands' (UIR bands), with principal members at 3.3, 6.2, 7.7, 8.6 and 11.3 μm, were first observed in the mid-IR towards NGC 7027 by Gillett, Forrest & Merrill (1973). Cohen et al. (1986, 1989) found good correlations between the strengths of all pairs of bands towards a sample of PNe, reflection nebulae and H II regions, showing that they correspond to a generic spectrum. The strength of the 7.7-μm feature relative to the total *IRAS* flux correlates strongly with the gas-phase C/O ratio in a sample of six PNe (Cohen et al. 1986), and Duley & Williams (1981) identified the principal wavelengths of the UIR bands with transitions in the chemical functional groups of aromatic molecules. Polycyclic aromatic hydrocarbons are the commonly accepted carriers for the UIR bands (Léger & Puget 1984). Thus, although their exact carriers still remain to be determined, the UIR bands are indicative of a carbon-rich environment.

The 8–13 μm spectra of PNe can also show significant continuum emission attributed to 'warm' dust at ~200 K. As first shown by Aitken et al. (1979), a smooth emission feature with a peak at about 9.7 μm is observed in the PNe SwSt 1, M 1-26 and Hb 12. The peak of emission coincides with the Si–O stretch in silicates (Day 1979, 1981), and this feature is similar to

★ E-mail: p.roche@physics.ox.ac.uk

amorphous condensates of silicate materials (Day & Donn 1978). It is typical of the Trapezium region in Orion and of the circumstellar shells of some oxygen-rich stars (Forrest, Gillett & Stein 1975), and is also seen in absorption towards the BN infrared point source in Orion (Gillett et al. 1975). Willner et al. (1979) detected a smooth emission feature with a rather flat profile, from 10.5 μm to about 12.7 μm, towards the PNe IC 418 and NGC 6572. It is commonly observed towards carbon stars as excess emission over a blackbody spectrum, and is attributed to lattice vibrations in silicon carbide (Forrest et al. 1975). Andersen et al. (1999) published the mid-IR transmission spectrum of meteoritic SiC grains; they obtained a good match to the C-star feature when extracting grains with a small size distribution (i.e., <5 μm).

There are thus significant compositional differences in the dust content of PNe, which can be classified into dust emission types, and according to whether they contain O-rich or C-rich grain materials (Aitken et al. 1979). How do the 10-μm dust emission features compare with the gas-phase abundances? What is the proportion of PNe that show each type of dust emission, and does their distribution show large-scale variations across the Galactic disc? It has been shown by Thronson et al. (1987) and Jura, Joyce & Kleinmann (1989) that the proportion of C stars relative to M giants increases outside the solar circle, and it is interesting to investigate whether PNe follow a similar trend. In contrast to the C and M stars which span a range of locations in the giant branch, PN compositions reflect the surface abundances at the end of the AGB, with a well-defined evolutionary status.

This paper is the first of a series devoted to the statistical analysis of the grain composition in Galactic disc PNe. In Section 2 we present a sample of 74 PNe with 8–13 μm spectra, which includes 24 previously unpublished spectra obtained with CGS3 on UKIRT or the UCL spectrometer on UKIRT or the AAT. Section 2 also contains a brief description of the method used to classify the 10-μm continua (following Aitken et al. 1979). We will then compare in Section 3 the dust content of PNe with their gas-phase C/O and N/O abundance ratios, to show that the dust emission types represent an alternative for determining the C/O chemical balance and bring complementary information on the PN progenitors. The sky distribution of PN dust types is presented in Section 4. After adopting a statistical distance scale in Section 5, we will test in Section 6 the size of the PN sample in this work for stratification in Peimbert (1978) types, and discuss its homogeneity, giving some support for its statistical significance. The Galactic disc distribution of the PN dust composition is presented in Section 7. Section 8 summarizes our conclusions.

2 8–13 μm SPECTROSCOPY OF COMPACT AND INFRARED-BRIGHT PNe

The criteria for selection of the PN sample were that they be compact, less than 10 arcsec in diameter so that most of the flux is contained in the spectrograph beam, and infrared-bright, with *IRAS* 12-μm flux in excess of 0.5 Jy. These criteria select the best candidates for the detection of the dust emission features. A sample of 10 PNe was observed with CGS3 on UKIRT on 1996 September 27 and 28, with the intention of increasing the number of objects measured beyond the solar circle. An observing log is presented in Table 1, where details of the previously unpublished spectra from the AAT and UKIRT are listed. Both CGS3 and the UCLS were used in their low-resolution modes, producing oversampled spectra which are calibrated with respect to standard stars. Fluxes are accurate to 20 per cent. The fluxes of emission lines present in some objects are listed in Table 2. Although they provide information on the ionized gaseous component, we will not use the emission lines for the purpose of this work. The resulting spectra are shown in Fig. 1, together with fits to the 8–13 μm continua based on the grain emissivities, which form the basis of the dust type classification.

We classified the type of dust emission features according to the procedure described in Aitken et al. (1979) and Aitken & Roche (1982). The emissivity functions ϵ_i for the three types of grains are taken from the spectra of astrophysical sources, with $F_\lambda = \epsilon_i B(\lambda, T)$, where F_λ is the observed flux density, and $B(\lambda,T)$ is a Planck function at temperature T [ϵ_i is then fixed by $\epsilon_i(10\,\mu\mathrm{m}) = 1$]. Additionally, a smooth continuum with emissivity $f(\lambda) \propto \lambda^{-1.8}$, which is taken to represent graphite grains (or

Table 1. Log of observations.

	l [degrees]	b	Instrument	Date
NGC 6537	10.01	0.70	UKIRT+CGS3	May 94
NGC 6578	10.80	−1.80	UKIRT+UCLS	Oct 87
M1-71	55.50	−0.50	UKIRT+UCLS	Jul 90
Hen2-447	57.90	−1.50	UKIRT+UCLS	Jul 90
K3-53	64.90	−2.10	UKIRT+UCLS	Jul 90
K3-52	67.90	−0.20	UKIRT+UCLS	Jul 90
M3-35	71.60	−2.30	UKIRT+UCLS	Jul 86
Hu1-2	86.50	−8.80	UKIRT+UCLS	Oct 87
M1-77	89.30	−2.20	UKIRT+CGS3	Sep 96
M2-49	95.10	−2.00	UKIRT+CGS3	Sep 96
K3-62	95.20	+0.70	UKIRT+UCLS	Jul 90
K3-60	98.20	+4.90	UKIRT+CGS3	Sep 96
Me2-2	100.00	−8.70	UKIRT+UCLS	Oct 87
Bl2-1	104.10	+1.00	UKIRT+CGS3	Sep 96
M2-54	104.80	−6.70	UKIRT+CGS3	Sep 96
K4-57	107.40	−0.60	UKIRT+CGS3	Sep 96
M1-4	147.40	−2.30	UKIRT+CGS3	Sep 96
IC 2149	166.10	+10.40	UKIRT+CGS3	Sep 96
K3-69	170.70	+4.60	UKIRT+CGS3	Sep 96
M1-5	184.00	−2.10	UKIRT+UCLS	Oct 87
M1-14	234.90	−1.40	UKIRT+CGS3	Sep 96
Hen2-117	320.90	+2.20	AAT+UCLS	Apr 87
Hen2-142	327.10	−2.20	AAT+UCLS	Apr 86
Pe1-7	337.40	+1.60	AAT+UCLS	Apr 86

Table 2. Emission-line fluxes, in $10^{-15}\,\mathrm{W\,m^{-2}}$.

	[Ar III] 8.99 μm	[S IV] 10.52 μm	[Ne II] 12.81 μm
NGC 6578	2.10	17.0	–
M1-71	3.57	5.52	2.27
Hen2-447	1.04	–	5.98
K3-53	–	2.56	–
K3-52	0.51	2.45	1.00
M3-35	–	4.77	1.99
Hu1-2	–	1.93	–
M1-77	–	–	0.98
M2-49	–	2.29	–
K3-62	1.16	2.36	0.58
K3-60	–	2.27	–
Me2-2	–	0.63	–
M2-54	–	–	0.90
M1-4	–	5.52	–
IC 2149	–	–	2.02
M1-14	0.89	–	1.33
Hen2-117	4.03	13.9	3.92
Hen2-142	–	–	11.8
Pe1-7	–	–	22.5

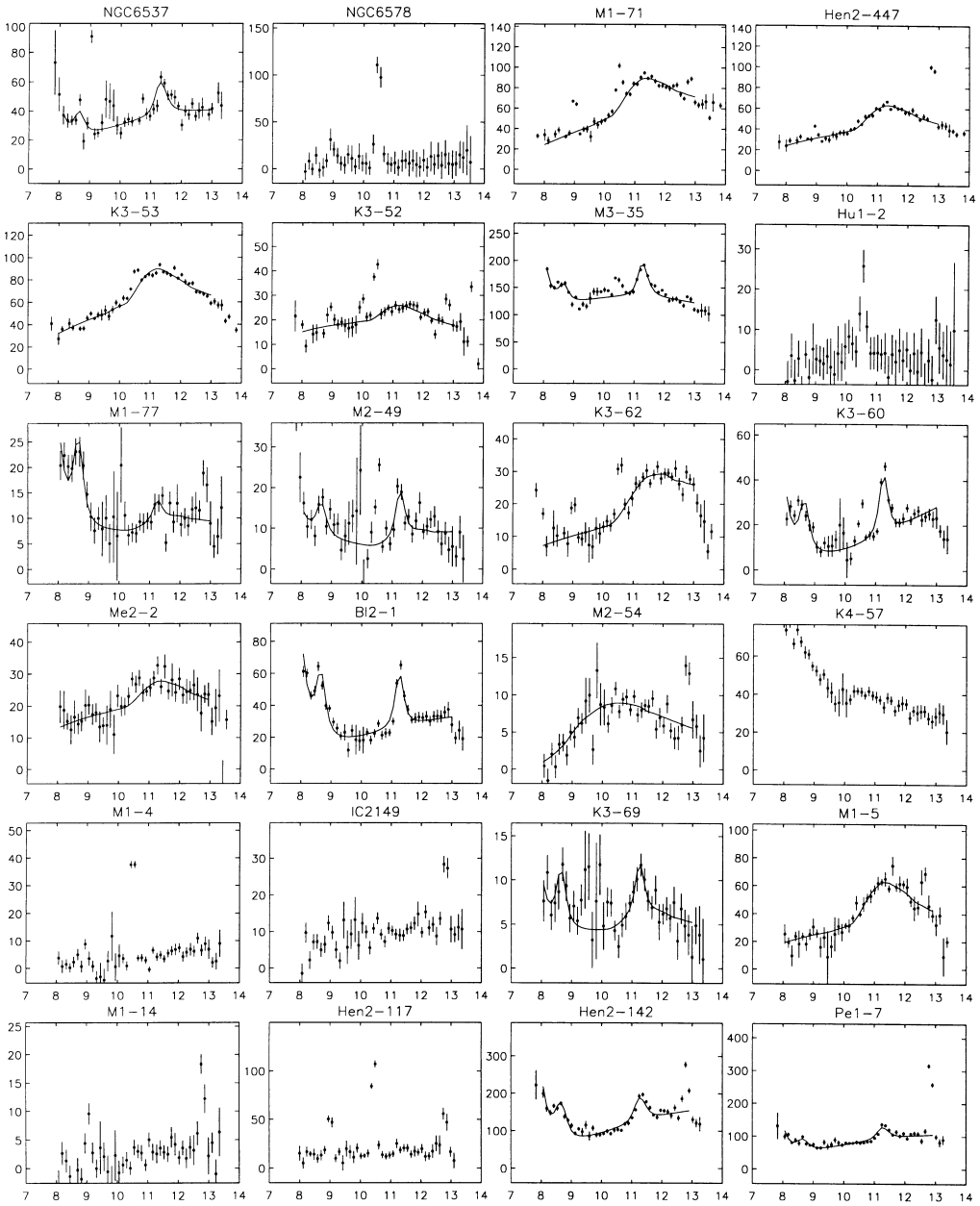

Figure 1. 10-μm spectra for the PNe listed in Table 1. In abscissae is the wavelength range in μm, and in ordinates the flux density in $10^{-19}\,\mathrm{W\,cm^{-2}\,\mu m^{-1}}$. A fit to the continuum emission is shown for the spectra with identified dust features, with parameters listed in Table 4. The data points around bright emission lines ([A III], [S IV] and [Ne II] at 8.99, 10.52 and 12.81 μm respectively) are excluded from the fits.

amorphous carbon grains), was included in the fitting procedure. The relative contribution of emissivity functions and the temperatures of the grains are fitted to the 8–13 μm continua, following a χ^2 minimization:

$$F_\lambda = \sum_i a_i \epsilon_i(\lambda) B(\lambda, T_i)/B(10\,\mu\mathrm{m}, T_i), \quad (1)$$

$$\chi^2 = \sum_\lambda (F_\lambda^{\mathrm{obs}} - F_\lambda)^2/\sigma_\lambda^2, \quad (2)$$

where the sum extends to the number of dust components used in the fit, and ϵ_λ stands for the error in each point of the observed spectrum F_λ^{obs}. The Planck functions are arbitrarily normalized at 10 μm. Best-fitting values are thus obtained for the measure of contribution of each emission type a_{1-4}, and their blackbody temperatures T_{1-4}. The relative contribution of each dust type is $a_i' = a_i/\sum_j a_j$, summing over all the dust types required in the fit. The coefficient a′ is thus a representation of the fractional emission at $\lambda = 10\,\mu$m. The fitting procedure assumes that all emitting materials are optically thin, and that any absorption occurs in a cold foreground layer; in the case of absorption a

Table 3. Classification of PN dust types.

O	(silicates)	Silicate grain emission.
C	(UIR)	UIR bands but not silicates.
c	(SiC)	SiC grains, but neither silicates nor the UIR bands.
+	(weak)	Weak or unidentifiable continuum.

Table 4. List of all PNe with 8–13 μm spectra, and the identified warm dust emission features.

name	*l*	*b*	dust type	ref. [a]	N/O type	He	C	N	O	ref. [h]	*D* Z95	*D* *IRAS*	comments
solar						0.10	3.6(−4)	9.3(−5)	7.4(−4)	24			
SwSt1	1.50	−6.70	O	3	III	0.11	3.9(−4)	4.1(−5)	5.9(−4)	1	3.79	4.12	silicates:0.95,203 UIR:0.05,2000
NGC 6369	2.40	5.80	+	4	I	0.13	5.8(−4)	1.2(−4)	2.9(−4)	2	0.75	3.96	weak continuum
Hb4	3.10	2.90	+	7	I	0.13	–	2.8(−4)	4.8(−4)	2	2.68	9.52	weak continuum
Hb6	7.20	1.80	+	7	I	0.11	–	4.5(−4)	5.1(−4)	2	2.45	6.99	weak continuum
NGC 6309	9.60	14.80	+	4	II	0.11	1.3(−3)	1.2(−4)	9.5(−4)	3	2.35	8.16	weak continuum
NGC 6537[i]	10.01	00.7	C	–	I	0.19	4.0(−5)	8.9(−4)	1.7(−4)	23	1.60	3.41	graphite:0.20,157 UIR:0.56,0.12,0.12[f]
NGC 6578	10.80	−1.80	+	–	II	0.11	–	1.1(−4)	5.6(−4)	2	2.47	3.93	weak continuum[e]
M2 − 9	10.80	18.00	O	3	III	0.08	–	5.0(−5)	2.3(−4)	4	3.01	2.82	thick-silicates:0.38,536,1.09 graphite:0.62,235
NGC 6741	33.80	−2.60	C	7	I	0.11	8.0(−4)	2.4(−4)	5.4(−4)	5	2.33	6.85	graphite:0.29,128 UIR:0.71,295
NGC 6572	34.60	11.80	c	3	II	0.09	1.3(−4)	9.6(−5)	3.1(−4)	6a	1.02	2.91	SiC:0.18,190 graphite:0.82,183
NGC 7009	37.70	−34.50	+	4	II	0.10	2.7(−4)	1.8(−4)	5.3(−4)	7	1.09	4.35	weak continuum
NGC 6790	37.80	−6.30	c	1	IIb	0.11	7.2(−4)	5.5(−5)	7.6(−4)	8	3.18	5.69	SiC:0.31,142 graphite:0.69,188
CN3 − 1	38.20	12.00	+	7	III	–	5.0(−4)	4.9(−5)	1.3(−4)	3	4.05	10.27	weak continuum
NGC 6210	43.10	37.70	+	4	IIb	0.10	–	4.9(−5)	5.0(−4)	3	1.73	6.84	weak continuum
Vy2-2	45.40	−2.70	O	3	I	0.09	–	4.4(−5)	2.7(−4)	4	7.93	3.93	silicates:0.95,365 SiC:0.03,100 graphite:0.02,111
Hu2-1	51.40	9.60	c	7	III	0.09	4.2(−4)	4.0(−5)	3.0(−4)	3	4.52	10.50	SiC:0.17,200 graphite:0.83,175
M1-71	55.50	−0.50	c	–	–	–	–	–	–	–	3.17	5.90	graphite:0.73,165 SiC:0.27,186
Hen2-447	57.90	−1.50	c	–	–	–	–	–	–	–	6.30	8.44	graphite:0.73,186 SiC:0.27,179
IC 4997	58.30	−10.90	O	3	III	0.13	4.1(−4)	2.0(−4)	1.2(−3)	6b	4.43	7.83	silicates:0.95,217 UIR:0.05,2000
NGC 6886	60.10	−7.70	C	7	II	0.09	4.1(−4)	1.3(−4)	3.1(−4)	9	3.13	10.67	graphite:0.22,132 UIR:0.78,355
BD + 303639	64.70	5.00	C	3	IIb	–	4.0(−4)	1.1(−4)	3.7(−4)	10	1.85	2.12	SiC:0.03,80 graphite:0.60,252 UIR:0.36,633
K3-53	64.90	−2.10	c	–	–	–	–	–	–	–	6.95	8.24	graphite:0.70,178 SiC:0.30,316
K3-52	67.90	−0.20	c	–	–	–	–	–	–	–	7.10	7.51	graphite:0.78,207 SiC:0.22,262
Hen2-459	68.30	−2.70	C	7	–	–	–	–	–	–	6.02	5.85	graphite:0.60,150 UIR:0.40,550
M3-35	71.60	−2.30	C	–	–	–	–	–	–	–	4.44	6.85	graphite:0.24,191 UIR[d]:0.57,0.07,0.12
NGC 6881	74.50	2.10	C	7	I	0.11	–	3.8(−4)	5.5(−4)	2	3.96	6.73	graphite:0.70,150 UIR:0.30,250
NGC 6884	82.10	7.00	+	7	IIb	0.10	1.0(−3)	3.0(−4)	1.0(−3)	11	2.63	9.23	weak continuum
NGC 6826	83.50	12.70	+	4	IIb	0.11	1.7(−3)	3.0(−5)	2.4(−4)	3	1.42	5.52	weak continuum
NGC 7027	84.90	−3.40	C	1	II	0.11	6.9(−4)	1.3(−4)	3.1(−4)	12	0.64	–	SiC:0.08,151 graphite:0.45,168 UIR:0.47,228
Hu1-2	86.50	−8.80	+	–	I	0.16	1.2(−4)	3.2(−4)	1.1(−4)	3	2.66	17.49	weak continuum
M1-77	89.30	−2.20	C	–	–	–	–	–	–	–	5.29	9.16	graphite:0.07,200 SiC:0.006,81 UIR[d]:0.64,0.22,0.06
IC 5117	89.80	−5.10	C	3	II	0.11	7.9(−4)	1.1(−4)	4.1(−4)	3	3.83	5.23	SiC:0.09,159 graphite:0.61,213 UIR:0.30,369
21282[g]	93.90	−0.10	C	8	–	–	–	–	–	–	10.53	3.38	prominent UIR bands
M2-49	95.10	−2.00	C	–	–	–	–	–	–	–	6.30	9.23	graphite:0.12,330 SiC:0.01,70 UIR[d]:0.34,0.2,0.31
K3-62	95.20	0.70	c	–	–	–	–	–	–	–	4.07	8.98	graphite:0.79,224 SiC:0.21,89
NGC 6543	96.40	29.90	+	4	IIb	0.11	1.3(−3)	8.7(−5)	5.6(−4)	3	1.12	3.36	weak continuum
K3-60	98.20	4.90	C	–	I	0.13	–	1.9(−4)	4.3(−4)	2	6.28	10.63	graphite:0.06,106 UIR[d]:0.59,0.17,0.18
Me2-2	100.00	−8.70	c	–	I	0.14	–	6.9(−4)	2.1(−4)	2	7.30	17.30	graphite:0.85,192 SiC:0.15,142
IC 5217	100.60	−5.40	+	7	–	–	–	–	–	–	–	–	weak continuum
Bl2-1	104.10	1.00	C	–	–	–	–	–	–	–	6.05	10.86	graphite:0.06,135 UIR[d]:0.64,0.18,0.12
M2-54	104.80	−6.70	O	–	–	–	–	–	–	–	13.80	11.45	silicates:1.0,173
K4-57	107.40	−0.60	+	–	–	–	–	–	–	–	–	–	unidentified
Hb12	111.80	−2.80	O	3	IIb	0.10	1.1(−4)	6.0(−5)	2.2(−4)	13	8.11	4.13	silicates:0.71,304 SiC:0.23,2000 graphite:0.05,2000
M2-56	118.40	8.42	O	3	–	–	–	–	–	–	–	2.69	thick-silicates:0.53,279,1.32 graphite:0.47,2000
M4-18	146.70	7.60	C	3	–	–	–	–	–	–	6.85	10.53	SiC:0.03,232 graphite:0.43,137 UIR:0.54,113
M1-4	147.40	−2.30	+	–	IIb	0.10	–	9.1(−5)	3.2(−4)	2	3.53	14.84	weak continuum
IC 2149	166.10	10.40	+	–	II	0.09	1.3(−4)	4.3(−5)	2.9(−4)	14	2.07	8.85	unidentified (graphite at 157K)
K3-69	170.70	4.60	C	–	–	–	–	–	–	–	25.50	23.23	graphite:0.11,200 SiC:0.02,108 UIR[d]:0.48,0.21,0.18
M1-5	184.00	−2.10	c	–	–	–	–	–	–	–	4.96	12.01	graphite:0.65,187 SiC:0.35,166
J900	194.20	2.50	C	3	IIb	0.12	2.0(−3)	4.3(−5)	3.9(−4)	15	3.40	11.04	graphite:0.34,143 UIR:0.66,133

Table 4 – *continued*

name	*l*	*b*	dust type	ref.[a]	N/O type	He	C	N	O	ref.[h]	*D* Z95	*D* *IRAS*	comments
NGC 2392	197.80	17.30	+	4	II	–	2.1(−4)	2.1(−4)	3.6(−4)	16	1.44	9.84	weak continuum
M1-6	211.20	−3.50	c	7	IIb	0.06	–	3.9(−5)	3.4(−4)	4	4.35	10.50	SiC:0.21,110 graphite:0.79,175
IC 418	215.20	−24.20	c	1	IIb	0.07	2.7(−4)	8.3(−5)	2.1(−4)	6c	1.02	2.62	SiC:0.26,120 graphite:0.74,200
IC 2165	221.30	−12.30	c	5	II	0.10	4.1(−4)	7.9(−5)	2.0(−4)	17	2.52	11.94	SiC[c]:-,- graphite:-,90
M1-11	232.80	−4.70	c	3	III	0.02	–	2.7(−5)	5.5(−5)	18	4.24	4.63	SiC:0.25,234 graphite:0.59,194
M1-14	234.90	−1.40	+	–	III	0.10	–	2.6(−5)	1.9(−4)	19	4.37	13.57	weak continuum (possible SiC)
M1-12	235.30	−3.90	c	7	III	0.02	–	3.2(−5)	1.3(−4)	18	6.48	10.11	SiC:0.24,140 graphite:0.76,210
NGC 3242	261.00	32.00	+	4	IIb	0.09	2.7(−4)	8.1(−5)	4.6(−4)	3	0.94	5.51	weak continuum
IC 2501	281.00	−5.60	c	3	II	0.11	6.1(−4)	1.6(−4)	5.1(−4)	1	2.12	7.10	SiC:0.17,137 graphite:0.83,202
Hen2-47	285.60	−2.70	O	3	IIb	0.03	–	2.3(−4)	1.2(−3)	4	3.08	5.66	silicates:0.66,242 graphite:0.34,143
IC 2621	291.60	−4.80	C	3	–	0.09	–	–	8.3(−4)	15	2.79	6.19	SiC:0.1,144 graphite:0.5,256 UIR:0.4,211
NGC 5315	309.10	−4.30	C	3	I	0.09	1.6(−3)	6.1(−4)	6.4(−4)	15	1.96	4.15	SiC:0.16,2000 graphite:0.55,271 UIR:0.29,125
Hen2-131	315.10	−13.00	O	3	III	–	1.4(−4)	1.8(−4)	4.7(−4)	1	2.20	3.89	silicates:0.42,409 graphite:0.58,162
Hen2-117	320.90	2.20	+	–	–	–	–	–	–	–	–	–	weak continuum (possible UIR)
Hen2-113	321.50	4.00	C	2	IIb	–	5.0(−3)	6.6(−5)	4.8(−4)	22	5.50[j]	1.95	UIR bands (like NGC 7027)
Hen2-142	327.10	−2.20	C	–	–	–	–	–	–	–	4.62	5.02	graphite:0.11,140 UIR[d]:0.64,0.16,0.09
HDE330036	330.80	4.10	C	6	I	–	1.9(−4)	2.4(−4)	2.3(−4)	20	–	5.05	UIR bands
Mz3	331.70	−1.00	O	3	I	0.18	–	3.5(−4)	2.8(−4)	16	1.17	1.84	thick-silicates:0.83,525,1.42 graphite:0.17,220
CPD-568032	332.92	−9.91	C	2	IIb	–	6.3(−3)	8.3(−5)	4.8(−4)	22	–	1.85	UIR bands (like NGC 7027)
Pe1-7	337.40	1.60	C	–	–	–	–	–	–	–	3.53[j]	3.89	graphite:0.18,152 UIR[d]:0.60,0.11,0.11
NGC 6302[i]	349.50	1.00	C	7	I	0.18	1.0(−4)	8.3(−4)	5.0(−4)	21	0.57	1.59	graphite:0.66,154 UIR:0.34,490
M1-26	358.90	−0.70	O	1	III	0.08	1.5(−4)	4.5(−5)	3.0(−4)	15	2.42	2.76	Silicates:1,201
19w32	359.20	1.20	O	7	–	–	–	–	–	–	4.30[j]	4.38	blackbody[b]:1,390,1.26
Hb5	359.30	−0.90	C	3	I	0.14	–	1.1(−3)	6.6(−4)	2	1.32	3.09	graphite:0.41,162 UIR:0.59,248

[a] The references for the 10-μm spectra are: (1) Aitken et al. 1979; (2) Aitken et al. 1980; (3) Aitken & Roche 1982; (4) Roche et al. 1983b; (5) Roche & Aitken 1983; (6) Roche et al. 1983a; (7) Roche & Aitken 1986; (8) Roche et al. 1991.

[b] Blackbody with optically thick foreground silicates with $\tau(10\,\mu\mathrm{m}) = 1.26$.

[c] Free–free, continuum-substracted SiC and graphite are required, but in a range of proportions and temperatures.

[d] The UIR bands were fitted using individual resonance profiles.

[e] The spectrum of NGC 6578 presented here, with little continuum, is in contrast with that obtained with the *IRAS* LRS (Kwok et al. 1986), which shows prominent silicate emission. Observations at UKIRT show that a star ∼30 arcsec to the SE of NGC 6578 has a silicate emission band which has probably contaminated the *IRAS* LRS spectrum.

[f] This CGS3 spectrum was obtained with a 4-arcsec beam, which may account for the relative weakness of the 11.3-μm feature compared to other nebulae (observed with 10-arcsec beams).

[g] IRAS 21282 + 5050. The radio data for the *S*(6)-cm-based distance was taken from Likkel et al. (1994).

[h] The references for the gas-phase abundances are: (1) Perinotto (1991); (2) Aller & Keyes (1987); (3) Aller & Czyzak (1983); (4) Köppen et al. (1991); (5) Hyung & Aller (1997); (6a) Hyung et al. (1994a); (6b) Hyung et al. (1994b); (6c) Hyung et al. (1994c); (7) Hyung & Aller (1995); (8) Aller et al. (1996); (9) Hyung et al. (1995); (10) Aller & Hyung (1995); (11) Hyung et al. (1997); (12) Keyes et al. (1990); (13) Hyung & Aller (1996); (14) Feibelman et al. (1994); (15) Kingsburgh & Barlow (1994); (16) Zuckerman & Aller (1986); (17) Hyung (1994); (18) Cuisinier et al. (1996); (19) Costa et al. (1996); (20) Lutz (1984); (21) Aller et al. (1981); (22) De Marco et al. (1997); (23) Feibelman et al. (1985); (24) Grevesse & Anders (1989).

[i] The C abundances listed for NGC 6302 and 6537 are probably underestimated: in NGC 6302, C v is the most abundant ion, but was not included by Aller et al. (1981). We adopted $C/O = 0.9$ for NGC 6302 (Professor M. Barlow, private communication), and did not use the C/O information for NGC 6537.

[j] Radio data from the Strasbourg-ESO catalogue, and references therein.

factor $e^{-\tau(\lambda)}$ is included in equation (2) [$\tau(\lambda)$ is the wavelength-dependent opacity, with a profile given by the emissivity curve, keeping $\tau(10\,\mu m)$ as a free parameter]. The available data provide insufficient constraints to warrant a more detailed radiative transfer treatment.

As discussed in Aitken & Roche (1982), it is the silicate grain emission feature that really separates PNe into different groups. A portion of PNe with silicate emission also show the UIR bands, and sometimes require SiC in small amounts. Graphite emission seems to be unrelated to the other types of grains. The PN dust signatures can be placed into four groups based on the dominant dust species at 10 μm, as shown in Table 3.

A list of all the identified dust emission features found in this sample of PNe can be found in Table 4. The S/N ratios of many spectra are rather low, and higher quality data may confirm the need for mixture of grain types. However, in this paper we are concerned with the dominant material. The column under 'comments' gives more information on the best-fitting parameters, in the form

$$(\text{graintype}) : a', T, \tau, \tag{3}$$

where the optical depth field τ is listed for only when absorption is required (which is the case for M2-9 only).

As would be expected from blackbody radiation between 8 and 13 μm, a typical dust temperature is $\gtrsim$200 K, and the 8–13 μm dust emission can be referred to as 'warm dust emission features' in comparison with colder dust $\lesssim$200 K which makes the bulk of the FIR emission (e.g. Kwok, Hrivnak & Milone 1986).

The objects are listed in the Strasbourg-ESO catalogue (Acker et al. 1992) as 'true or probable' PNe. The exception is IRAS 21282+5050, whose optical spectrum (Cohen & Jones 1987) shows [O III] emission lines, photospheric absorption features corresponding to a heavily reddened [WC 11] nucleus, and a total luminosity of about $2 \times 10^3\,L_\odot$ for an estimated distance of 2 kpc, making it a probable low-excitation PN (the central star has been re-classified as an O star by Crowther, De Marco & Barlow 1998).

In the notation of Table 3, out of 74 Galactic disc PNe with 8–13 μm spectra, there are 12 O nebulae (of which SwSt1 and IC 4997 also show the UIR bands and Hb12 shows SiC emission), 16 c nebulae and 26 C nebulae (for nine of which the fits are improved with the inclusion of SiC). The remainder shows either too little continuum emission (17 PNe), or no clear identification in terms of the classification used here (e.g., IC 2149 and M1-14 whose spectra are best fitted by graphite emisssion only, and K4-57, whose spectrum is flat in units of Janskys, and is atypical of PNe).

3 COMPARISON OF THE DUST COMPOSITIONS AND THE GAS-PHASE ABUNDANCES

How does the warm dust emission feature classification, based on the grain C/O chemical balance, compare with the gas-phase C/O abundance ratios? How does it compare to nitrogen enrichment? In order to address these questions, we searched the literature for published gas-phase abundances in PNe with 8–13 μm spectra. Table 4 lists the PNe for which a detailed spectroscopic analysis is available, but it should be borne in mind that the uncertainties in the abundance analysis are often substantial. The PNe are classified according to the Peimbert (1978) types, with the subtypes in N/O ratio introduced by Faúndez-Abans & Maciel (1987). Many assignments to N/O types are taken from the compilation in Maciel & Dutra (1992).

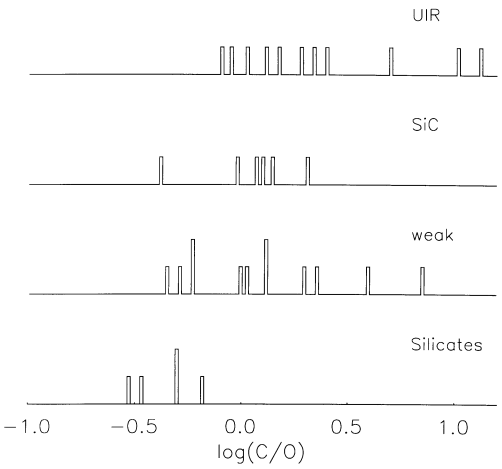

Figure 2. Histogram showing the number of nebulae of each dust type as a function of gas-phase C/O ratios. Typical error bars are $\sim$+0.11/−0.15 horizontally for a 20 per cent uncertainty in the abundance calculations.

Fig. 2 shows the distribution of gas-phase C/O ratios for each 8–13 μm continuum class. The correspondence is not direct; some nebulae with C-based grains have gas-phase C/O < 1. There is, however, a good correlation in C-based grains with C/O ratio, previously obtained by Barlow (1983) and Roche (1989), for example, but with a lower number of PNe. Silicate grains indicate an O-rich environment, SiC a C-rich environment, and the UIR bands correlate with a strong overabundance of C relative to O. Weak continuum PNe are widely spread in C/O ratios, suggesting they may correspond to later evolutionary stages, rather than C/O $\sim$ 1. It is established that the dust grain composition reflects on average the gas-phase composition, and can be used as probes of C enrichment in PNe. The warm dust features are thus an alternative to the UV lines [C II] λ2326, [C III] λ1908 and [C IV] λ1550 for coarse classifications of C/O ratios.

The existence of five PNe with C/O < 1 and grain emission characteristic of C-rich environments merits further attention. The same apparently paradoxical situation is hinted at by the superposition of silicates and C-based grains in the spectra of SwSt1, IC 4997 and Hb12 (confirmed by measurements at 3 μm showing the 3.3-μm UIR band; Roche et al. 1996). Standard equilibrium chemistry suggests the least abundant of C or O would be locked in CO (Gilman 1969), and the production of C-rich molecules in O-rich circumstellar environments may be a rather rare non-equilibrium phenomenon (observed towards certain M supergiants in h and χ Per; Sylvester, Skinner & Barlow 1998). This is also suggested by the appearance of both C- and O-type grains in novae (e.g. Smith et al. 1995). Thus, mixtures of grain types imply either a stratification in the ejecta composition of the progenitor star, or the mixing of the progenitor ejecta with pre-existing material. This point is relevant when linking the grain types with the C/O ratios of the progenitor stars, and will be discussed further in a forthcoming paper (Casassus & Roche 2001, hereafter Paper II).

The link between the dust types and N enrichment is shown in Fig. 3. The UIR bands are found mostly in nebulae of Peimbert type I, whereas SiC emission and 'weak' continuum PNe are uniformly represented. Silicates are found either with strong N enrichment (type I), or none at all (types IIb and III). These trends

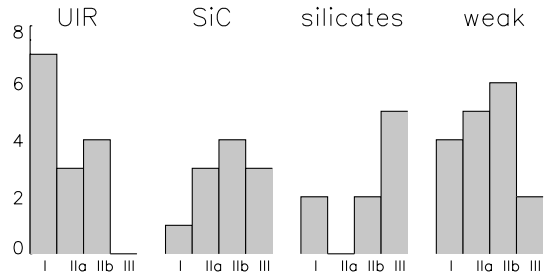

Figure 3. Relative proportion of PN dust types among Peimbert (1978) types, with subtypes from Faúndez-Abans & Maciel (1987).

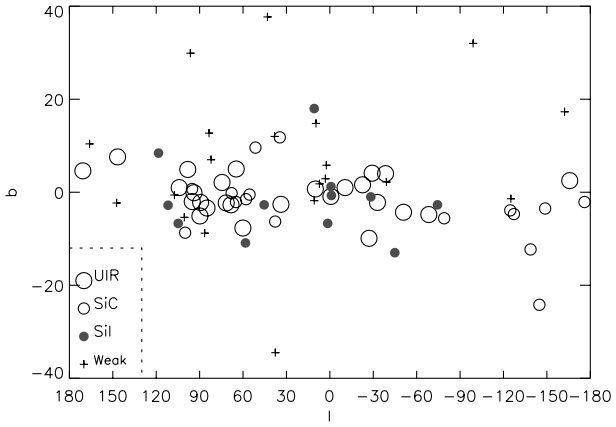

Figure 4. Sky distribution of PN dust types.

Table 5. The properties of the sky distribution of planetary nebulae dust types. The errors quoted correspond to one standard deviation.

	$\langle b \rangle$ [degrees]	$b_{\rm rms}$ [degrees]	N	$l < 90$ $l > 270$	$90 < l$ $l < 180$
O	-1.6 ± 2.3	8.0 ± 1.6	12	9	3
c	-3.3 ± 2.0	7.9 ± 1.4	16	8	8
C	-0.4 ± 0.8	4.1 ± 0.6	26	19	7
+	6.6 ± 3.5	15.5 ± 2.5	20	12	8

should be confirmed with a larger sample of objects with known N/O ratios, especially for O-type signatures.

The stratification of PNe in N/O ratios with height above the Galactic plane suggests that the Peimbert classification is indicative of progenitor mass. Thus, on a relative mass scale, the UIR bands correspond to higher progenitor masses, and SiC to intermediate masses; silicates are found mainly for low-mass progenitors, but also for the most massive ones. The uniform distribution of 'weak' continuum PNe again suggests they may correspond to later evolutionary stages.

However, the dichotomy between O- and C-type PNe for high gas phase N/O abundance ratios indicates that there is no simple correspondence between progenitor mass and dust signature. The dust emission features provide complementary information to the Peimbert types.

4 THE SKY DISTRIBUTION OF PN DUST TYPES

The sky distribution of PN dust types, built using Table 4, is shown in Fig. 4. Table 5 contains the moments of the distribution. We assumed that the main source of errors on the fraction of each dust type is due to 'counting noise', and the uncertainties in the mean $\langle b \rangle$ and spread $b_{\rm rms}$ are estimated under the assumption that the parent distribution of PN latitudes is normal.

The mean $\langle b \rangle$ is reasonably close to the Galactic plane for all identified dust types. The much larger spread in 'weak' PNe suggests they are closer on average; a larger spread in height above the plane is discarded on the basis that 'weak' PNe are uniformly distributed in Peimbert types, although the adoption of a distance scale is required to discuss this issue further. It seems that UIR PNe are the most concentrated towards the Galactic plane, although SiC and silicate PNe have roughly the same spread in galactic latitude. For the subset of PNe with C-based grains (the SiC and UIR nebulae), $b_{\rm rms} = 6.0 \pm 0.7$, giving the ratio of the spreads for O-rich PNe to C-rich PNe, $b_{\rm rms}({\rm O})/b_{\rm rms}({\rm C}) = 1.3 \pm 0.3$. All uncertainties quoted in this paper are $\pm 1\sigma$.

There is a hint of a decrease in the proportion of silicate grains PNe from the first and fourth quadrants ($-90° < l < 90°$) to the second and third quadrants ($90° < l < 270°$), from 0.25 ± 0.07 to 0.17 ± 0.09. Since this corresponds to only 1σ, it cannot be considered a solid property of the distribution. There is also an indication of an increase in the relative proportion of SiC PNe, which doubles from 0.22 ± 0.07 to 0.44 ± 0.11.

5 ADOPTED DISTANCE SCALES

5.1 Distance scales based on 6-cm continuum emission

One of the persistent problems related to the study of PNe is the difficulty of obtaining accurate distances. A review of the methods based on individual properties of PNe can be found in Peimbert (1992). These so-called 'direct' distance estimators are available for a restricted number of objects, and suffer from intrinsic uncertainties. However, the distances to PNe can be determined on a statistical basis, which match the average properties of PNe. A distance scale for PNe can be built on the assumption that a general relationship holds for a set of PNe. We adopted the distance scale derived by Zhang (1995), who used an arithmetic average of two complementary methods, one based on the mass–radius relationship (see, e.g., the review by Kwok 1994), and the other on the relationship between $T_{\rm b}$, the free–free 6-cm brightness temperature, and nebular radius (as introduced by Van de Steene & Zijlstra 1994). Zhang (1995) calibrated the mass–radius and $T_{\rm b}$–radius relationships with a large sample of PNe with individually and 'directly' determined distances. This 'direct' method is explained in detail by Zhang (1993) and Zhang & Kwok (1993), and depends on the distance-independent parameters $T_{\rm b}$ and the central star temperature T_*. Distances thus obtained are strongly model-dependent, and are often in disagreement with the more accurate comparison of angular expansion rate and radial velocity. However, the details of the distances to each nebula are of secondary importance as long as the global properties of PNe are reproduced. In that sense, the Zhang (1995) distance scale gives a Gaussian distribution about the Galactic Centre for bulge PNe, with a narrower scatter than the scale by Van de Steene & Zijlstra (1994).

5.2 Distances from *IRAS* fluxes to optically thick PNe

As the central stars of PNe evolve rapidly in time, and the nebulae are active radiatively and dynamically (e.g. Kwok 1994), distance

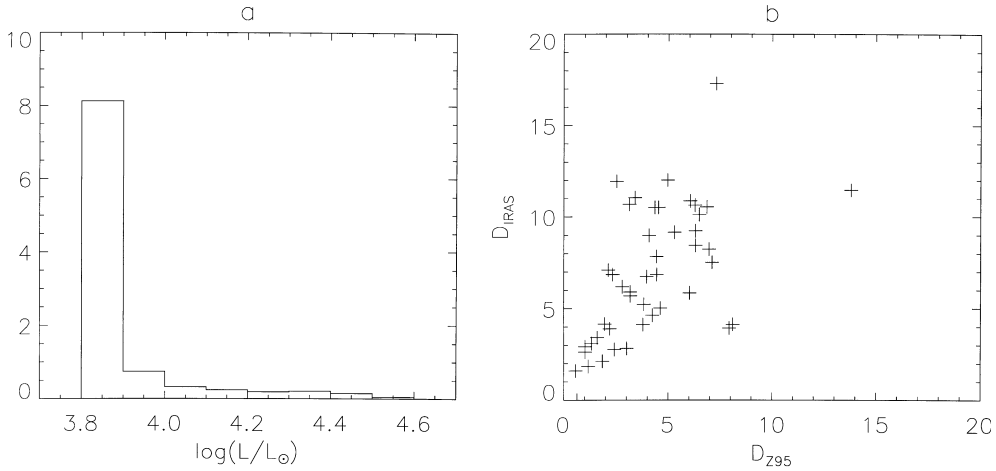

Figure 5. (a) Synthetic PNe luminosity function from the initial–final mass relationship of Groenewegen & de Jong (1993), and with progenitor ZAMS masses between 1.2 and 7 $M_\odot$. (b) The relationship between D_{IRAS} and Zhang (1995) for the PNe with warm dust emission.

scales based on invariant properties of PNe cannot be applied to the whole PNe population. However, in the case of the sample discussed here, the four *IRAS* band fluxes, coupled with constant luminosity, may provide an alternative distance scale, as we now argue.

The compact and IR-bright PNe are likely to be young, surrounded by substantial molecular material and therefore optically thick to the ionizing radiation from the central star. In this case, the total luminosity of the nuclei can be inferred from the flux of any H I recombination line, by equating the number of H^+ recombinations to the number of photoionizations. Méndez, Kudritzki & Herrero (1992) tested this hypothesis by comparing with spectroscopic studies of PNe nuclei, linking the surface gravity and effective temperature to the luminosity through atmosphere models. Their conclusion is that most PNe are optically thin. However, their sample is biased against obscured central stars: out of 23 PNe, six are IR-bright and are among the sample discussed here, four of which have no warm dust. Thus Méndez et al. included only two nebulae with 8–13 μm spectra showing warm dust emission, for which the ratio of luminosities derived from optical thickness to the model-atmosphere luminosities are 0.70 and 0.92 (for M1-26 and IC 418). It is thus likely that the compact and IR-bright PNe with warm dust emission are optically thick.

In PNe which are optically thick in the Lyman continuum, the ionized central regions are surrounded by substantial amounts of neutral gas, an environment favourable to dust-grain survival. Most of the UV radiation escaping from the ionized region would be absorbed by dust grains, which heat up as a result to ∼100–200 K, and re-radiate in the mid- and far-IR spectral ranges. The *IRAS* band fluxes should give a good representation of the bolometric fluxes using

$$F_{IRAS} = \sum_{j=1}^{4} \nu I_\nu(j), \tag{4}$$

where the sum extends to the four *IRAS* bands.

PNe initially evolve at a constant luminosity once they leave the AGB, as was first shown by Paczyński (1970; see also Blöcker 1995). The luminosity function for the youngest PNe should be close to that of tip-of-the-AGB objects. The distribution of core masses for stars at the tip of the AGB can be calculated with a synthetic AGB model and a crude Galactic disc model (we used the analytic prescriptions in Groenewegen & de Jong 1993, and a Galactic disc model described in Paper II). The core-mass luminosity relationship from Wagenhuber & Groenewegen (1998), in the case of post-AGB objects (i.e., in the asymptotic regime and vanishing envelope mass), gives the luminosity function of young PNe[1] shown in Fig. 5(a), with a mean of 8500 $L_\odot$. A very similar luminosity function, with an average of 9300 $L_\odot$, is obtained using the prescriptions of Wagenhuber & Groenewegen, and taking solar metallicity and an IMF index of 1 (instead of 1.72 in Paper II, in a notation where the Salpeter 1955 IMF would be 1.35) with a constant star formation rate.

It appears the PN luminosities are not expected to vary over more than one order of magnitude. Assigning the same luminosity of 8500 $L_\odot$ for all PNe gives a maximum error on the distance of only a factor $\lesssim$2. Distances to compact and IR-bright PNe can thus be estimated under the assumption of constant luminosity. Equation (4) for the bolometric flux is likely to be a lower limit only, but in this paper we are interested in the relative properties of the distribution of the different PNe dust types, and their absolute distances are not required. We will refer to distances derived in this way as D_{IRAS}, and those from Zhang (1995) as D_{Z95}.

We stress that D_{IRAS} distances are only meant to investigate an independent distance scale and its consequences on the derived Galactocentric trends; these distances should not be taken as accurate.

5.3 Adopted distances to compact and IR-bright PNe

The distances derived from the two methods described above are listed in Table 4. D_{IRAS} distances appear to be reasonable for PNe with detected warm dust emission. Fig. 5(b) shows a good correlation between the two distance estimates in the case of PNe with warm dust emission. For PNe with warm dust emission, the ratio D_{IRAS}/D_{Z95} is 1.87 on average, with a 1σ spread of 0.84. This suggests that the luminosity used to derive D_{IRAS} distances may be overestimated by a factor of ∼ 3–4, if D_{Z95} distances are reliable.

D_{IRAS} may be used as an upper limit, except for PNe with upper limits in the *IRAS* 100-μm band. The PNe Vy2-2,

[1] PNe progenitors for the sample discussed here were assumed to have masses in the range $1.2 < M/M_\odot < 7$; see Paper II.

IRAS 21282+5050, Hb12 and Hen2-113 are given distances on the Zhang (1995) scale that are in excess of D_{IRAS} by a factor larger than 1.7 (which takes into account the maximum range expected in the PNe luminosity function). In the remainder of this paper we assign D_{IRAS} distances to PNe without radio data (i.e., M2-56 and HDE330036).

The case of K 3-69 seems to be anomalous: both distance estimates give ∼25 kpc, putting K 3-69 at 1.7 kpc above the Galactic plane, and we preferred to use the distance of 7.9 kpc from Cahn, Kaler & Stanghellini (1992). Another anomalous case is M2-54: again, the Zhang (1995) distance scale and D_{IRAS} both give a distance of ∼13 kpc, placing it near the northern Galactic warp. In order to avoid the uncertainties associated with exaggeratedly large distances, we adopted a maximum Galactocentric radius of 14 kpc to compute the moments of the vertical distribution, thus excluding K 3-69 and M 2-54.

6 TESTS FOR THE COMPLETENESS AND HOMOGENEITY OF THE COMPACT AND IR-BRIGHT PN SAMPLE

The sequence in Peimbert (1978) types is indicative of progenitor mass, the highest being associated with type I. There is a stratification in height above the Galactic plane as a function of N/O type (e.g. Maciel & Dutra 1992). Such a stratification is indeed present in this sample. Inside the solar circle, the root mean square height over the plane, $z_{\rm rms}$, is 0.14 kpc for type I, 0.37 for type IIa, 0.45 for type IIb, and 0.68 for type III. This stratification is an indication that a statistical study based on the compact and IR-bright PN sample would be sensitive to PN properties with the same dependence on progenitor mass as the Peimbert types. Out of 49 compact and IR-bright PNe with known N/O ratio, 29 ± 6 per cent are type I, 21 ± 6 per cent are type IIa, which is typical of PN catalogues (e.g. Maciel & Dutra 1992). The disc PN population seems to be homogeneously sampled, although the constraints will remain loose until a larger sample is available.

A discussion of the selection effects is possible in terms of a comparison between the fraction of O-rich PNe and the predictions of synthetic AGB models. In Paper II we find that for a minimum PNe progenitor mass of 1 $M_\odot$, about 50 per cent of all young PNe should be O-rich, whereas we report 22 per cent. The minimum PNe progenitor mass for the sample in this work is $M^{\rm min} = 1.2$, at a 2σ confidence level.

The good agreement between D_{IRAS} and D_{Z95} suggests equation (4) can be used to estimate the fraction of luminosity radiated in the 12-μm *IRAS* band by PNe with warm dust emission, with

$$\frac{L_{12\,\mu\rm m}}{L_*} = \frac{\nu I\nu(12\,\mu\rm m)}{\sum_{j=1}^{4} \nu I_\nu(j)}. \qquad (5)$$

Omitting the PNe with upper limits in the 100-μm *IRAS* band, the fraction of luminosity emitted at 12 μm is ∼ 0.25 ± 0.15 for PNe with silicate emission, 0.22 ± 0.09 for SiC PNe, 0.27 ± 0.14 for UIR PNe, and ∼0.25 ± 0.14 for all warm dust types[2] ('weak' PNe have a $L_{12\,\mu\rm m}/L_*$ ratio of 0.11 ± 0.03). Considering the relatively large uncertainties, the above values show that, for a given central star luminosity, the IR-bright selection criterion would not preferentially select one type of grains above others (at least in broad terms).

[2] This sample is biased towards high values of $L_{12\,\mu\rm m}/L_*$, so the average for all PNe would be much lower.

At a lower flux limit of 0.5 Jy, and under the assumption that 20 per cent of the total luminosity is radiated in the 12-μm *IRAS* band, the Galactic disc should be fully sampled: the maximum distance at which a PN with warm dust would be detected is 20 kpc, for $L_* = 10\,000\,L_\odot$.

It is thus apparent that the completeness and homogeneity of the sample discussed here are dominated by the selection effects in the PNe catalogues themselves. As PNe are, for the most part, discovered through optical surveys, the distances are unlikely to be much in excess of 3 kpc, especially towards the inner Galaxy.

7 THE GALACTIC DISC DISTRIBUTION OF PNe DUST EMISSION FEATURES

The spatial distribution of PNe dust types can now be constructed using Table 4, and is shown in Fig. 6 in the case of the Zhang (1995) distance scale. Table 6 lists the properties of the distribution. The total number of sources is $N_{\rm tot} = 54$, consisting of 33 for $R < R_0$, and 21 for $R > R_0$ ($R_0 = 8.5$ kpc; Kerr & Lynden-Bell 1986). The decrease in the relative proportion of silicate PNe, which was hinted at in Section 4, is confirmed to a somewhat higher degree of significance: the fraction of silicate PNe decreases from 0.27 ± 0.08 for $R < R_0$ to 0.14 ± 0.08 for $R > R_0$. There is a concentration of UIR PNe towards $z = 0$, confirming that they are related to higher progenitor masses. On the other hand, SiC and silicate nebulae have a similar spread in height above the Galactic plane. However, the vertical distribution of PN dust types is rather homogeneous when compared to that obtained in the Peimbert types.

Table 7 summarizes the properties of the PNe distribution obtained with D_{IRAS} distances. It might seem surprising that SiC nebulae are at greater distances on average, but this is compatible with finding most SiC nebulae outside the solar circle, where PN catalogues are less affected by extinction. The proportion of silicate PNe is confirmed to decrease with R at a higher degree of significance: the fraction of silicate PNe decreases from 0.32 ± 0.09 for $R < R_0$ to 0.14 ± 0.06 for $R > R_0$.

As is apparent from Fig. 6, 'weak' nebulae are closer on the Zhang (1995) scale. It was mentioned that PNe with no warm dust are equally distributed among Peimbert types, and that their gas-phase C/O ratios reflect the proportions for the whole sample. They also have higher 6-cm fluxes, which together with the selection criteria of compact angular size, explains why they are on average closer on the Zhang (1995) scale. It is thus very likely that PNe with weak continuum correspond to later evolutionary stages, and are not a transition stage where C/O ∼ 1. Although D_{IRAS} distances are not applicable to 'weak' PNe, whose optical thickness is uncertain, it is interesting to note that the average D_{IRAS} distance to 'weak' PNe is 9.0 kpc, greater than for any other type of PNe. This could be interpreted as a lower average luminosity (as expected for more evolved PNe on the white dwarf cooling track), or that for 'weak' PNe the far-IR flux F_{IRAS} is not a good approximation to the bolometric flux.

There is a peculiar asymmetry in the face-on distribution of PNe in Fig. 6. The sector of the Galactic disc with southern galactic longitudes (the third and fourth quadrants) is underpopulated. This effect is due simply to the incompleteness of the catalogues. The same asymmetry can be seen in the face-on map of Durand, Acker & Zijlstra (1998), with a larger number of PNe. Warm dust PNe with reliable *IRAS* fluxes all gather in very tight IRAS colour–colour boxes (in particular, in a

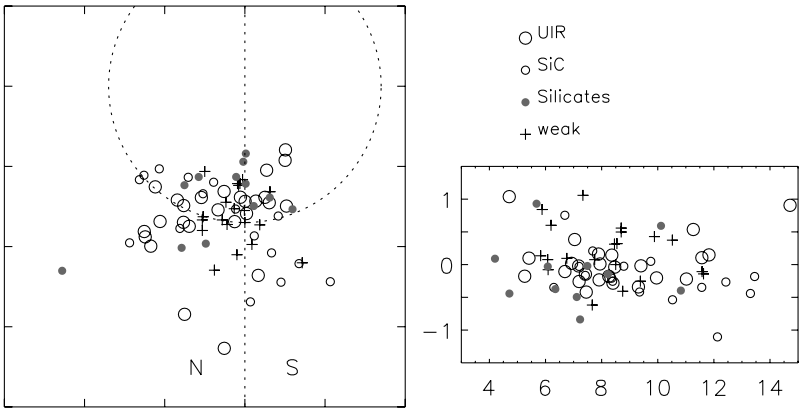

Figure 6. The Galactic disc distribution of dust emission types in PNe, with distances from Zhang (1995). Left: Face-on view of the disc (ticks every 5 kpc, the solar circle is shown in dashed line). Right: Vertical distribution, in kpc.

Table 6. The properties of the distribution of planetary nebulae dust types, based on the distances from Zhang (1995). The errors quoted correspond to one standard deviation.

	$D/D_{\rm rms}$ [kpc]	$\langle z\rangle$ [100 pc]	$z_{\rm rms}$ [100 pc]		N $<R_0$	$>R_0$
O	3.9/2.1	-1.0 ± 1.4	4.7 ± 1.0	12	9	3
c	4.3/2.0	-1.8 ± 1.0	4.1 ± 0.7	16	7	9
C	3.8/2.3	-0.0 ± 0.5	2.3 ± 0.3	26	17	9
+	2.3/1.0	2.3 ± 0.9	4.7 ± 0.8	19	10	9

Table 7. Same as Table 6, but with D_{IRAS} distances.

	$D/D_{\rm rms}$ [kpc]	$\langle z\rangle$ [100 pc]	$z_{\rm rms}$ [100 pc]		N $<R_0$	$>R_0$
O	4.0/1.6	-1.8 ± 1.9	6.2 ± 1.3	12	8	4
c	8.4/3.6	-4.6 ± 2.7	11.0 ± 1.9	16	4	12
C	5.6/3.2	-0.7 ± 0.9	4.4 ± 0.6	26	13	13

$\log[F(100\,\mu{\rm m})/F(60\,\mu{\rm m})]$ versus $\log[F(25\,\mu{\rm m})/F(12\,\mu{\rm m})]$ plot) which allows the selection of all warm-dust PNe candidates from the *IRAS* PSC. We found 331 *IRAS* point sources with colours of warm-dust PNe, whose galactic longitude/latitude distribution is fairly uniform from northern to southern longitudes. Also, the Carina spiral arm between the third and fourth quadrants is viewed tangentially from the Sun, thus increasing the interstellar extinction and limiting the PN discovery rate.

8 CONCLUSIONS

The total number of PNe with 8–13 μm spectra has been increased to 74 with the inclusion of 24 new objects. The sample consists of all compact and IR-bright PNe listed in the Strasbourg-ESO catalogue. 54 PNe have clearly identified warm dust emission features, which are placed into three groups: 12 PNe show silicate emission, 16 show SiC, and 26 show the UIR bands. The remainder have 8–13 μm spectra dominated by emission lines, and correspond to later evolutionary stages. Thus 22 ± 6 per cent of the PNe with warm dust emission have O-rich grains. We have used this sample for an initial study of the PNe dust emission features in the Galactic context.

A comparison of the PNe dust types with the gas-phase C/O ratio shows a good correspondence: Silicate nebulae have $C/O < 1$, and SiC nebulae are found with $C/O \gtrsim 1$, while PNe that show the UIR bands often have $C/O \gg 1$. We thus confirm that the dust emission features represent an alternative to the plasma diagnostic for measuring the C/O chemical balance in PNe. Nebulae that show the UIR emission bands also have the highest N/O gas-phase ratio. Silicate nebulae are found either with high N/O ratios, or with no nitrogen enrichment at all. On the other hand, SiC nebulae are more uniformly distributed in N/O ratios. Thus, on a relative mass scale, PNe with emission from the UIR bands correspond to higher progenitor masses, and those with SiC to intermediate masses. Silicates are found mainly for low-mass progenitors, but also for the most massive ones. The dust emission features thus provide complementary information on the progenitors masses to the Peimbert types.

The adoption of statistical distances for PNe confirmed that the sample is large enough to show stratification in Peimbert types. The link between objects with UIR band emission and higher progenitor masses is confirmed through their concentration towards the Galactic plane, obtained from their sky distribution and through the use of two independent PNe distance scales. There is a trend for a decreasing proportion of O-rich PNe with Galactocentric radius, confirmed by both distance scales, from 30 ± 9 per cent inside the solar circle, to 14 ± 7 per cent outside. This trend reflects the variations in the M/C star ratio from Thronson et al. (1987) and Jura et al. (1989).

We also showed that the *IRAS* fluxes are a good representation of the bolometric flux for compact and IR-bright PNe, which are probably optically thick. The requirement $F(12\,\mu{\rm m}) > 0.5$ Jy should probe the whole Galactic disc, and the dominant selection effects are rooted in the PNe catalogues. Although all known IR-bright and compact PNe were included in this study, further observations are required to improve the statistics. Large-aperture telescopes and mid-IR array detectors will be much more sensitive for the detection of the warm dust emission features in these compact objects, and could allow a more accurate analysis.

ACKNOWLEDGMENTS

We are grateful to PATT for the time allocation on UKIRT, which is operated by the Joint Astronomy Centre on behalf of the Ppaper Physics and Astronomy Research Council, and PATT and ATAC for allocations on the AAT. SC acknowledges support from Fundación Andes and PPARC through a Gemini studentship. We acknowledge a very useful report from the referee.

REFERENCES

Acker A., Ochsenbein F., Stenholm B., Tylenda R., Marcout J., Schohn C., 1992, The Strasbourg-ESO Catalogue of Galactic planetary Nebulae. European Southern Observatory

Aitken D. K., Roche P. F., 1982, MNRAS, 200, 217

Aitken D. K., Roche P. F., Spenser P. M., Jones B., 1979, ApJ, 233, 925

Aitken D. K., Barlow M. J., Roche P. F., Spenser P. M., 1980, MNRAS, 192, 679

Aller L. H., Czyzak S. J., 1983, ApJS, 51, 211

Aller L. H., Hyung S., 1995, MNRAS, 276, 1101

Aller L. H., Keyes C. D., 1987, ApJS, 65, 405

Aller L. H., Ross J. E., O'Mara B. J., Keyes C. D., 1981, MNRAS, 197, 95

Aller L. H., Hyung S., Feibelman W. A., 1996, PASP, 108, 488

Andersen A. C., Jäger C., Mutschke H., Braatz A., Clément D., Henning Th., Jørgensen U. G., Ott U., 1999, A&A, 343, 933

Barlow M. J., 1983, in Flower D. R., ed., Proc. IAU Symp. 103, Planetary Nebulae. Reidel, Dordrecht, p. 105

Blöcker T., 1995, A&A, 299, 755

Cahn J. H., Kaler J. B., Stanghellini L., 1992, A&AS, 94, 399

Casassus S., Roche P. F., 2001, MNRAS, 320, 435 (Paper II, this issue)

Cohen M., Jones B. F., 1987, ApJ, 321, L151

Cohen M., Allamandola L., Tielens A.G.G.M., Bregman J., Simpson J. P., Witteborn F. C., Wooden D., Rank D. M., 1986, ApJ, 302, 737

Cohen M., Tielens A.G.G.M., Bregman J., Witteborn F. C., Rank D. M., Allamandola L. J., Wooden D. H., de Muizon M., 1989, ApJ, 341, 246

Costa R. D. D., Chiapini C., Maciel W. J., de Freitas Pacheco J. A., 1996, A&AS, 116, 249

Crowther P. A., De Marco O., Barlow M. J., 1998, MNRAS, 296, 367

Cuisinier F., Acker A., Köppen J., 1996, A&A, 307, 215

Day K. L., 1979, ApJ, 234, 158

Day K. L., 1981, ApJ, 246, 110

Day K. L., Donn B., 1978, ApJ, 222, L45

De Marco O., Barlow M. J., Storey P. J., 1997, MNRAS, 292, 86

Duley W. W., Williams D. A., 1981, MNRAS, 196, 269

Durand S., Acker A., Zijlstra A., 1998, A&AS, 132, 13

Faúndez-Abans M., Maciel W. J., 1987, A&A, 183, 324

Feibelman W. A., Aller L. H., Keyes C. D., Czyzak S. J., 1985, Proc. Nat. Acad. Sci., 82, 2202

Feibelman W. A., Hyung S., Aller L. H., 1994, ApJ, 426, 653

Forrest W. J., Gillett F. C., Stein W. A., 1975, ApJ, 195, 423

Gillett F. C., Forrest W. J., Merrill K. M., 1973, ApJ, 183, 87

Gillett F. C., Jones T. W., Merrill K. M., Stein W. A., 1975, A&A, 45, 77

Gilman R. C., 1969, ApJ, 155, L185

Grevesse N., Anders E., 1989, in Waddington C. J., ed., AIP Conf. Proc. 183, Cosmic Abundances of Matter. AIP, New York, p. 1

Groenewegen M. A. T., de Jong T., 1993, A&A, 267, 410

Hyung S., 1994, ApJS, 90, 119

Hyung S., Aller L. H., 1995, MNRAS, 273, 257

Hyung S., Aller L. H., 1996, MNRAS, 278, 551

Hyung S., Aller L. H., 1997, MNRAS, 292, 71

Hyung S., Aller L. H., Feibelman W. A., 1994a, MNRAS, 269, 975

Hyung S., Aller L. H., Feibelman W. A., 1994b, ApJS, 94, 465

Hyung S., Aller L. H., Feibelman W. A., 1994c, PASP, 106, 745

Hyung S., Keyes C. D., Aller L. H., 1995, MNRAS, 272, 49

Hyung S., Aller L. H., Feibelman W. A., 1997, ApJS, 108, 503

Jura M., Joyce R. R., Kleinmann S. G., 1989, ApJ, 336, 924

Kerr F. J., Lynden-Bell D., 1986, MNRAS, 221, 1023

Keyes C. D., Aller L. H., Feibelman W. A., 1990, PASP, 102, 59

Kingsburgh R. L., Barlow M. J., 1994, MNRAS, 271, 257

Köppen J., Acker A., Stenholm B., 1991, A&A, 248, 197

Kwok S., 1994, PASP, 106, 344

Kwok S., Hrivnak B. J., Milone E. F., 1986, ApJ, 303, 451

Léger A., Puget J. L., 1984, A&A, 137, 5

Likkel L., Morris M., Kastner J. H., Forveille T., 1994, A&A, 282, 190

Lutz J. H., 1984, ApJ, 279, 714

Maciel W. J., Dutra C. M., 1992, A&A, 262, 271

Méndez R. H., Kudritzki R. P., Herrero A., 1992, A&A, 260, 329

Paczyński B., 1970, Acta Astron., 20, 47

Peimbert M., 1978, in Terzian Y., ed., Proc. IAU Symp. 76, Planetary Nebulae. Reidel, Dordrecht, p. 233

Peimbert M., 1992, in White R. E., ed., Observational Astrophysics. IOP Publishing Ltd.

Perinotto M., 1991, ApJS, 76, 687

Roche P. F., 1989, in Torres Peimbert S., ed., Proc. IAU Symp. 131, Planetary Nebulae. Kluwer, Dordrecht, p. 117

Roche P. F., Aitken D. K., 1983, MNRAS, 203, 9

Roche P. F., Aitken D. K., 1986, MNRAS, 221, 63

Roche P. F., Allen D. A., Aitken D. K., 1983a, MNRAS, 204, 1009

Roche P. F., Aitken D. K., Whitmore B., 1983b, MNRAS, 204, 1017

Roche P. F., Aitken D. K., Smith C. H., 1991, MNRAS, 252, 282

Roche P. F., Lucas P. W., Hoare M. G., Aitken D. K., Smith C. H., 1996, MNRAS, 280, 924

Salpeter E. E., 1955, ApJ, 121, 161

Smith C. H., Aitken D. K., Roche P. F., Wright C. M., 1995, MNRAS, 277, 259

Sylvester R. J., Skinner C. J., Barlow M. J., 1998, MNRAS, 301, 1083

Thronson H. A., Latter W. B., Black J. H., Bally J., Hacking P., 1987, ApJ, 322, 770

Van de Steene G. C., Zijlstra A. A., 1994, A&AS, 108, 485

Wagenhuber J., Groenewegen M. A. T., 1998, A&A, 340, 183

Willner S. P., Jones B., Puetter R. C., Russell R. W., Soifer B. T., 1979, ApJ, 234, 496

Zhang C. Y., 1993, ApJ, 410, 239

Zhang C. Y., 1995, ApJS, 98, 659

Zhang C. Y., Kwok S., 1993, ApJS, 88, 137

Zuckerman B., Aller L. H., 1986, ApJ, 301, 772

This paper has been typeset from a TEX/LATEX file prepared by the author.